JOURNAL OF GEOPHYSICAL RESEARCH, VOL. 115, D01111, doi:10.1029/2009JD012512, 2010

Interaction of interannual and diurnal variations over equatorial Africa

Vasubandhu Misra[1,2]

Received 18 May 2009; revised 25 September 2009; accepted 30 September 2009; published 15 January 2010.

[1] This paper shows evidence of interannual variation of the local diurnal variability over equatorial Africa. The dry season of December–February over the equatorial African region of the eastern Democratic Republic of Congo (formerly Zaire) typically experiences wetter (drier) than normal seasonal anomalies during warm (cold) El Niño–Southern Oscillation (ENSO) events. This study finds that from the additive influence or phase locking of the seasonal cycle, the interannual signal from ENSO, and the local diurnal cycle, there is a tendency for local amplification of the remote ENSO signal over this region of equatorial Africa. This additive influence of the three temporal scales over the equatorial African region is established from the analysis of a multidecadal coupled ocean-atmosphere model integration that simulates the observed seasonal cycle and its interannual variations over equatorial Africa reasonably well.

Citation: Misra, V. (2010), Interaction of interannual and diurnal variations over equatorial Africa, *J. Geophys. Res.*, *115*, D01111, doi:10.1029/2009JD012512.

1. Introduction

[2] The focus of this paper is on a region largely located over the Democratic Republic of Congo (formerly Zaire; 20°E–30°E, 6°S–7°N). Hereafter, this region will be specifically referred to as equatorial Africa. This region has been selected to demonstrate the scale interactions across two very different spatial and temporal scales: local diurnal variability and large-scale interannual variations. There have been some scale interaction studies conducted in the frequency domain, pioneered by *Hayashi* [1980]. These studies compute wave energy flux across frequencies by examining, for example, the genesis and maintenance of the intraseasonal variability [*Krishnamurti et al.*, 2003], tropical middle-latitude interactions [*Krishnamurti et al.*, 1998], and dynamics of phase locking [*Krishnamurti and Chakraborty*, 2005]. This study, however, differs by showing the modulation of the local diurnal scale by the large-scale interannual variations without invoking an energy budget study of nonlinear interactions in frequency space.

[3] In many observational and modeling studies of African rainfall [*Nicholson*, 1986; *Nicholson and Kim*, 1997; *Mulenga et al.*, 2003; *Reason and Jagadeesha*, 2005; *Giannini et al.*, 2008], it is shown that the strongest El Niño–Southern Oscillation (ENSO) signals in Africa are prevalent over eastern equatorial Africa and southeastern Africa. Furthermore, many of these studies indicate that the rainfall signal over Africa is seasonally specific, which results in the signals being out of phase between the southern and equatorial latitudes of Africa. *Reason and Rouault* [2002] showed that ENSO-like decadal patterns of mean sea level pressure and sea surface temperature (SST) have considerable influence on the summer rainfall over eastern and northern South Africa on decadal time scales, which are also impacted by ENSO on interannual time scales. In this study, we show evidence of similar interaction across temporal scales, but between interannual variation of ENSO and local diurnal variability over equatorial Africa. In another related study, *Nicholson et al.* [1997] indicated that interannual variations of evapotranspiration can be significant over equatorial Africa with even zonal means of evapotranspiration varying by over 200 mm yr^{-1} over a long-term mean of the order of 350 mm yr^{-1}. *Balas et al.* [2007] showed in their observational work that there is considerable spatial heterogeneity in the interannual variations of precipitation over western equatorial Africa. *Jackson et al.* [2009] indicated that the interaction of topographic effects, the associated regional circulation, and the influence of the African easterly jet may partially explain for the spatial heterogeneity of the interannual variations over the western equatorial African region.

[4] *Hirst and Hastenrath* [1983] and *Lough* [1986] first showed connections between eastern Atlantic SST and rainfall over tropical Africa. *Nicholson and Entekhabi* [1987] showed the observed relationship between the eastern Atlantic SST along the coast of Angola and precipitation over equatorial Africa at interannual time scales. They found that this remote linkage comes from the modulation of the South Atlantic high and the Atlantic trades in response to the SST anomalies in the eastern Atlantic Ocean. In another related study, *Rouault et al.* [2003] showed that intrusion of warm water in the southeast Atlantic resulted in an increase in local convection and regional circulation anomalies. They suggest that this tele-

[1]Department of Meteorology, Florida State University, Tallahassee, Florida, USA.
[2]Center for Ocean-Atmospheric Prediction Studies, Florida State University, Tallahassee, Florida, USA.

0148-0227/10/2009JD012512$09.00

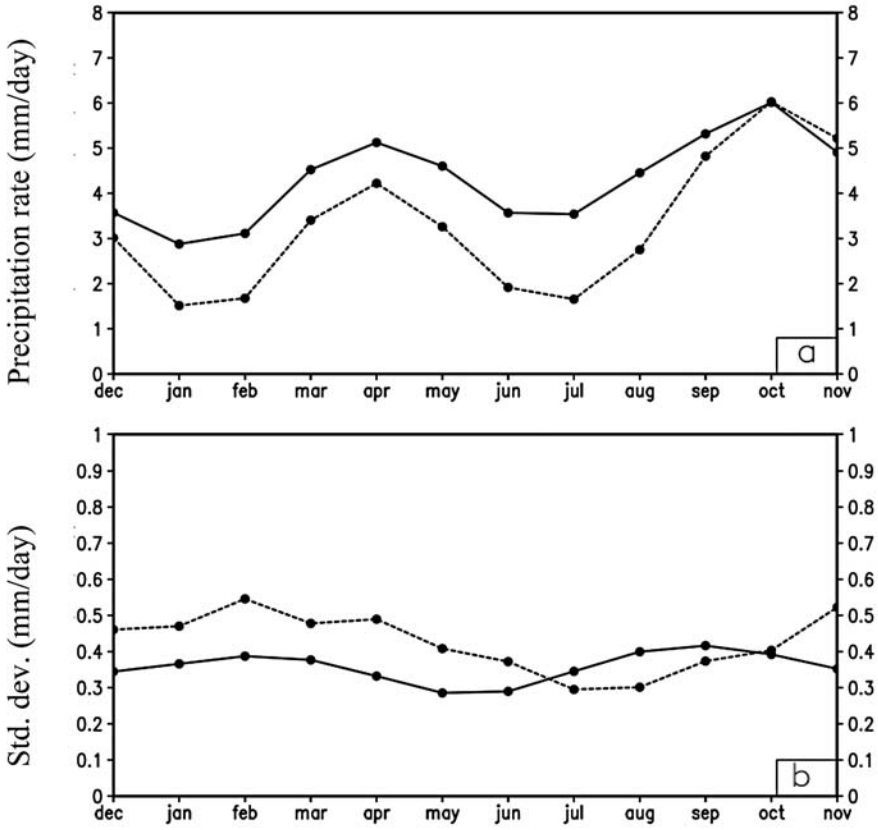

Figure 1. (a) The climatological seasonal cycle of precipitation over equatorial Africa from observations (Climate Research Unit (CRU); solid line) and the Center for Ocean-Land-Atmosphere Studies (COLA) coupled climate (CCC) model (dashed line). (b) Same as Figure 1a but for standard deviation.

connection is most robust when these local circulation anomalies modulate the flux of moisture from the Indian Ocean and southeasterly flux away from Africa toward the southeast Atlantic. *Hastenrath et al.* [1993] and *Kabanda and Jury* [1999] found that the ENSO-forced SST anomalies in the Indian Ocean can modulate the shorter rainy season over eastern equatorial Africa, which exhibits a double peak in its seasonal cycle. In a recent study, *Krishnamurthy and Kirtman* [2003] claimed that the SST variations in the western Indian Ocean are strongly correlated to the equatorial Pacific Ocean SST at interannual time scales, which further strengthens previous observations of the links between precipitation over equatorial Africa and SSTs in the neighboring western Indian Ocean and the remote eastern Pacific Ocean.

[5] This paper is organized as follows: a brief description of the climate model used in this study and a description of the model experiment are provided in section 2. The results are presented in section 3, followed by concluding remarks in section 4.

2. Model and Experiment Description

[6] The Center for Ocean-Land-Atmosphere Studies (COLA) coupled climate (CCC) model [*Misra et al.*, 2007; *Misra and Marx*, 2007] is used in this study. It consists of the atmospheric general circulation model (AGCM) version 3.2 at a spectral resolution of T62 with 28 sigma levels, identical to that of the National Centers for Environmental Prediction–National Center for Atmospheric Research (NCEP-NCAR) reanalysis model [*Kalnay et al.*, 1996]. The dynamical core follows from the Eulerian core of the community climate model version 3 [*Kiehl et al.*, 1998], wherein the dependent variables are spectrally treated, except for moisture, which is advected by a semi-Lagrangian scheme. The relaxed Arakawa-Schubert scheme [*Moorthi and Suarez*, 1992; *Bacmeister et al.*, 2000] is used for deep convective parameterization. The longwave and shortwave radiation schemes are identical to those in the community climate system model version 3.0 [*Collins et al.*, 2006]. The clouds are diagnosed following the work of *Slingo* [1987], and the cloud optical properties follow work by *Kiehl et al.* [1998]. The planetary boundary layer is a nonlocal scheme [*Hong and Pan*, 1996], and the shallow convection uses the formulation of *Tiedtke* [1984]. The land surface scheme uses the Simplified Simple Biosphere scheme (SSiB) [*Xue et al.*, 1991, 1996; *Dirmeyer and Zeng*, 1999].

[7] The COLA AGCM is coupled to the modular ocean model version 3.0 (MOM3) [*Pacanowski and Griffies*, 1998]. MOM3 covers the global oceans between 74°S and 65°N with realistic bottom topography. However, ocean depths less than 100 m are set to 100 m, and the maximum depth is set to 6000 m. The artificial high-latitude zonal

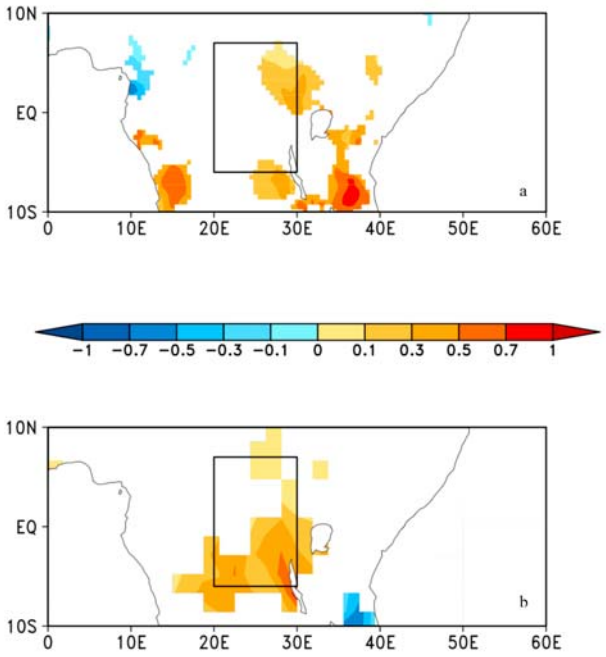

Figure 2. The contemporaneous regression of the December–January–February (DJF) seasonal mean precipitation from (a) the CRU and (b) the CCC model on the normalized Niño3 SST index from Hadley Center Global Sea Ice and Sea Surface Temperature (HADISST; Figure 2a) and the CCC model (Figure 2b). The units are in mm d^{-1}. The domain of equatorial Africa used in the study is outlined. Only significant values at the 90% confidence interval according to the *t* test are plotted. The regressions are scaled to one standard deviation of the Niño3 SST index. The equatorial Africa region is outlined.

boundaries are impermeable and insulating. MOM3 has a uniform zonal resolution of 1.5° whereas the meridional resolution is 0.5° between 10°S and 10°N, gradually increasing to 1.5° at 30°N and 30°S, and fixed at 1.5° in the extratropics. The vertical mixing is the nonlocal K profile parameterization of *Large et al.* [1994]; the momentum mixing is the space-time dependent scheme of *Smagorinsky* [1963]; and the tracer mixing follows the quasi-adiabatic stirring of *Redi* [1982] and *Gent and McWilliams* [1990].

[8] The CCC model is integrated for a period of 100 years from well spun-up ocean initial conditions that were obtained from a previous multidecadal coupled integration from the same coupled model. However, the results are presented from the last 50 years of the integration, when the surface meteorological variables were stored at intervals of 3 h.

[9] ENSO variability is of critical importance in this study. The fidelity of this variation in the CCC model has been discussed extensively by *Misra et al.* [2007]. *Misra et al.* [2007] showed that the CCC model is able to capture the seasonal phase locking of the ENSO variability to a realistic annual cycle of the eastern equatorial Pacific Ocean and that the model durations of the ENSO events are comparable to those of observations. Furthermore, the ENSO evolution in the CCC model conforms to the delayed oscillator theory. The model, however, has a relatively weaker ENSO variability than the observed variability and is dominated by the erroneous split Intertropical Convergence Zone (ITCZ) phenomenon.

3. Results

[10] For verification of the model results, precipitation from the Climate Research Unit (CRU) of the University of East Anglia [*Mitchell et al.*, 2004], available as a monthly mean at 0.5° from 1901 to 2000 for the global land surface, is used. Additionally, the Tropical Rain Measuring Mission 3B42 (TRMM) precipitation product is also used. This product is composed of 3-hourly derived precipitation rates from 1998 to the present at a horizontal resolution of 0.5°. Hadley Center Global Sea Ice and Sea Surface Temperature version 1.1 (HADISST) [*Rayner et al.*, 2003] is used for observed SSTs, which are available as monthly means at 1° resolution from 1901 to the present. A 6 year high-pass Butterworth filter is applied to CRU and HADISST data sets to remove variability on time periods longer than the interannual time scales [*Karspeck and Cane*, 2002]. The decadal variations in the CCC model data set are extremely small. The CO_2 concentration in the CCC model is kept at a constant value of 345 ppm to reflect the present-day concentrations. Therefore, the high-pass filter is not applied to the CCC model output data.

[11] For verification of the land-atmosphere interactions, the Global Offline Land Data assimilation (GOLD) [*Dirmeyer and Tan*, 2001] is used. It is available at daily time intervals for the period of 1960–2002 at T62 spectral truncation, which is ~200 km grid resolution. The land surface model in GOLD is SSiB, which is identical to that in the CCC model. There are 12 vegetation types in SSiB. The spatially varying soil parameters and spatiotemporally varying vegetation parameters are prescribed from the International Satellite Surface Climatology Project (ISLSCP) Initiative I land surface data set [*Meeson et al.*, 1995]. GOLD is forced by the meteorological forcing data from ERA-40 reanalyses and monthly precipitation estimates from the Global Precipitation Climatology Centre [*Rudolf et al.*, 1994]. GOLD was created to generate a spatially and temporally continuous land surface data set for specifying initial and/or boundary conditions for the CCC model and climate variability analysis over land. Some of the drawbacks of GOLD are that it is an uncoupled (with the atmosphere) integration of the land surface scheme and that it is forced with the NCEP-NCAR [*Kalnay et al.*, 1996] reanalysis surface meteorology, a model product that has errors from shortcomings in model resolution, parameterizations, and assumptions in the data assimilation. However, GOLD uses a number of gridded observational data sets at lower temporal resolution to help constrain the NCEP-NCAR reanalysis. The details of these observational data sets are given by *Dirmeyer and Tan* [2001]. It is also important to mention that the GOLD analysis is conducted with a land surface model that lacks a lake model. Given the proximity of Lakes Tanganyika and Victoria to our region of interest, this may be one of the significant limitations of the GOLD analysis.

3.1. Seasonal Cycle of Precipitation

[12] The seasonal cycle of precipitation over equatorial Africa from the CRU and the CCC model is shown in

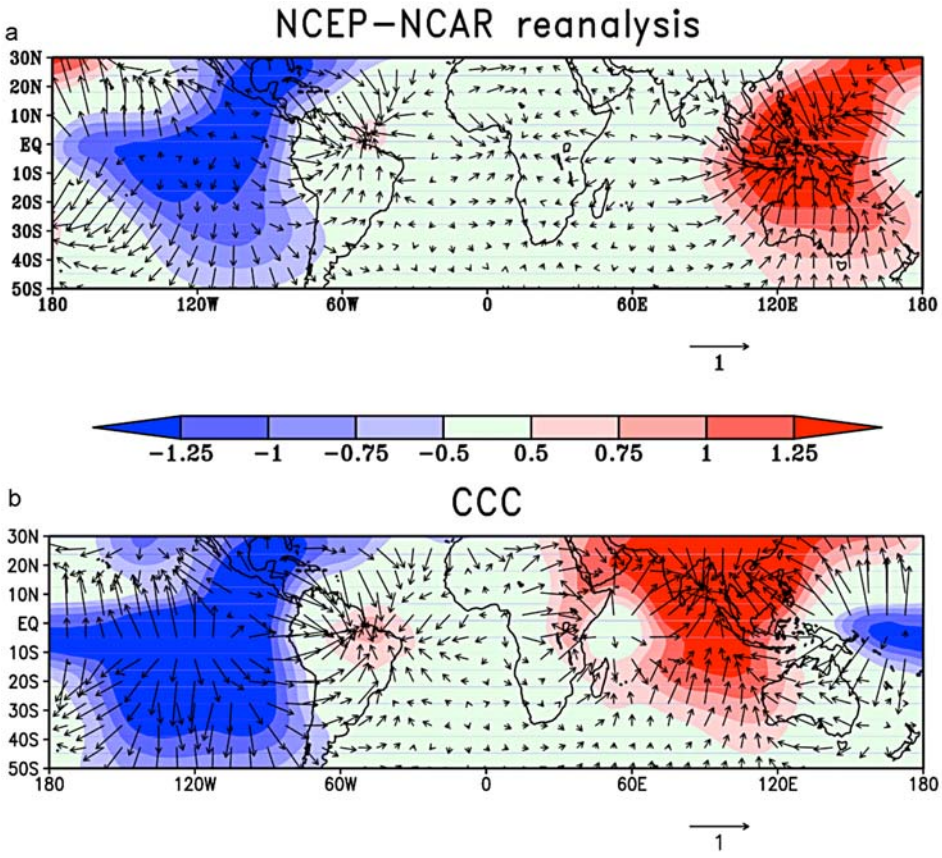

Figure 3. The regression of the mean DJF velocity potential (shaded) and divergent wind (vectors) at 200 hPa on the corresponding standardized Niño3 SST index from (a) the NCEP-NCAR reanalysis and (b) the CCC model. The unit of velocity potential (wind) is 1.0×10^{-6} m^2 s^{-1} (m s^{-1}). Velocity potential significant at 10% significance according to the t test is plotted. The regressions are scaled to one standard deviation of the Niño3 SST index.

Figure 1a. The observations in Figure 1a indicate that there are two distinct rainy seasons: one in March–May and the other in September–November, with the latter reaching the annual peak. The CCC model simulates the seasonal cycle of precipitation over equatorial Africa reasonably well and shows the double peak in the correct months of the year. However, the CCC model exhibits a relatively small dry bias in the seasonal cycle. The interannual variation of the observed precipitation (Figure 1b) over this region is not phase locked to this unique seasonal cycle. The standard deviation of the monthly mean observed precipitation is relatively "flat" with a modest increase in the late boreal winter season. These features of interannual variation of precipitation are also fairly well simulated in the CCC model. The CCC model, however, has a bias of overestimating the interannual variation of precipitation over the equatorial Africa region for most of the year, except in late boreal summer and fall seasons.

[13] The analysis in this paper will dwell on the December–January–February (DJF) season. This boreal winter season of DJF is unique to the equatorial Africa region for at least two reasons: it is the driest in the seasonal cycle of precipitation over the equatorial Africa region, and it is when the ENSO-forced variations peak.

3.2. Large-Scale Interannual Variation

[14] In Figure 2a, the regression of the DJF seasonal mean precipitation over equatorial Africa from CRU on the corresponding Niño3 SST index from HADISST is shown. It is clearly seen in Figure 2a that significant precipitation anomalies that appear over equatorial Africa correspond to wet (dry) precipitation anomalies during warm (cold) ENSO events. Figure 2b shows the corresponding CCC model. The CCC model is able to reasonably simulate these observed seasonal precipitation anomalies over equatorial Africa that are linearly related to the SST variability in the Niño3 region. There is, however, some apparent discrepancy in the simulated precipitation anomalies of the CCC model near the eastern coast of southern Tanzania. *Kijazi and Reason* [2005] showed that ENSO influence over the Tanzanian coast manifests over the intraseasonal scales. The error over Tanzania in Figure 2b is consistent with *Misra* [2009], who indicated that the CCC model has an erroneously low variance at intraseasonal time scales. Nonetheless, such remote teleconnection patterns are a result of the setting up of an anomalous atmospheric circulation in response to the SST anomalies [*Alexander et al.*, 2002; *Nigam*, 2003]. As *Gill* [1980] showed, for an equatorial heat source with a sinusoidal heating anomaly in the vertical, the atmospheric

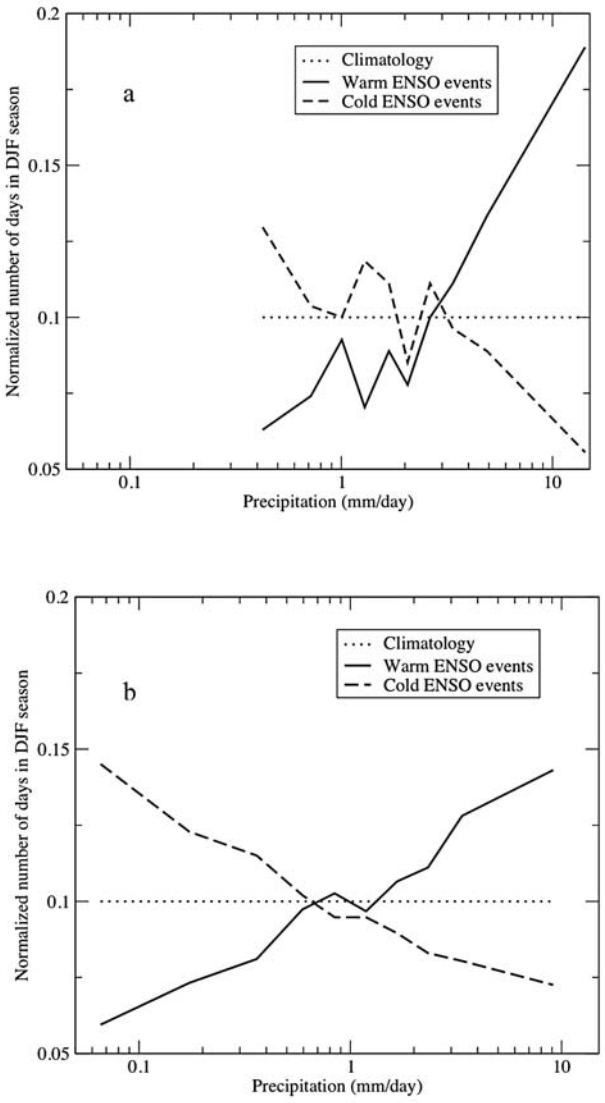

Figure 4. The daily rainfall distribution from (a) TRMM and (b) the CCC model over equatorial Africa.

response is the first baroclinic mode with a pair of anticyclones symmetric about the equator. The shifting of the deep tropical heating to the central equatorial Pacific region in a warm ENSO event leads to a consequent response of the atmosphere as shown in Figure 3. Figure 3 depicts the regression of the 200 hPa DJF seasonal mean divergence and divergent wind from the NCEP-NCAR reanalysis [*Kalnay et al.*, 1996] on the contemporaneous HADISST Niño3 SST index. Figure 3b shows the corresponding CCC model integration. There are obvious differences in the large-scale upper level anomalous divergence pattern between the NCEP-NCAR reanalysis (Figure 3a) and the CCC model (Figure 3b), especially in the strong upper level convergence over the Indo-Pacific region. During a warm ENSO event, the anomalous upper level convergence cell (with low-level divergence) is located farther westward in the CCC model compared to the NCEP-NCAR reanalysis. This is a result of the erroneous westward extension of the ENSO variability in the CCC model beyond the dateline, evident from the westward extension of the anomalous upper level divergence over the equatorial Pacific Ocean. This error is present in many of the coupled climate models [*Capotondi et al.*, 2006]. The associated secondary anomalous upper level divergence cell (with low-level convergence) over the western Indian Ocean is erroneously stronger in the CCC model relative to the NCEP-NCAR reanalysis. It is, however, this east-west anomalous atmospheric circulation that teleconnects the precipitation variability over equatorial Africa to remote SST variations over the Niño3 region in the eastern equatorial Pacific Ocean at interannual time scales. This can be noted from the close proximity of the precipitation anomalies over equatorial Africa in Figure 2 to the nodal point of the anomalous upper level divergent wind over the western Indian Ocean in both observations and in the model simulation. However, the differences observed in the anomalous atmospheric circulation between the NCEP reanalysis and in the CCC model in Figure 3 are consistent with the differences in the precipitation anomaly seen between the CRU data set and the CCC model simulation in Figure 2.

[15] This shift in the large-scale atmospheric circulation associated with ENSO variability also influences the distribution of the daily precipitation in the DJF season over the equatorial Africa region. This is shown in Figures 4a and 4b, which display the distribution of the daily precipitation normalized by the total number of days in the DJF season through the length of the data set in TRMM (8 years) and in the CCC model (50 years), respectively. They are binned into 10 unequal bins so that the respective climatological distribution over equatorial Africa has an equal number of days in each bin (decile; represented by the flat line at 0.1 in Figure 4). Both TRMM (Figure 4a) and the CCC model (Figure 4b) show a clear shift at the tail ends of the distribution between the warm and the cold ENSO events. It is apparent from Figure 4 that a cold (warm) ENSO event entails a higher frequency of stronger (weaker) precipitation events over equatorial Africa in both the CCC model and in the TRMM data sets. For example, in a La Niña year in Figure 4b, the CCC model simulates, on average, about 50% of the days in the DJF season having less than 1 mm d^{-1} of precipitation (obtained roughly as the area between the climatological distribution and the La Niña distribution up to 1 mm d^{-1}). Similarly, in an El Niño year, Figure 4b suggests that nearly 50% of the days in the DJF season have precipitation in excess of 1 mm d^{-1}. In comparison, TRMM observations indicate that nearly 50% of the days in the DJF season receive precipitation less than 2 mm d^{-1} in a La Niña year, whereas 50% of the days in an El Niño year receive over 3 mm d^{-1}. In other words, it may be noted that the CCC model clearly underestimates (overestimates) the strong (weak) precipitation events relative to TRMM during warm (cold) ENSO events. But the comparatively smaller sample size and higher spatial resolution of the TRMM data sets may have caused some of these differences from the CCC model in Figure 4.

3.3. Interannual Variation of the Diurnal Variability

[16] The interannual variation of the DJF seasonal precipitation anomalies over equatorial Africa shown in Figure 2 is comparable when the seasonally averaged daily diurnal

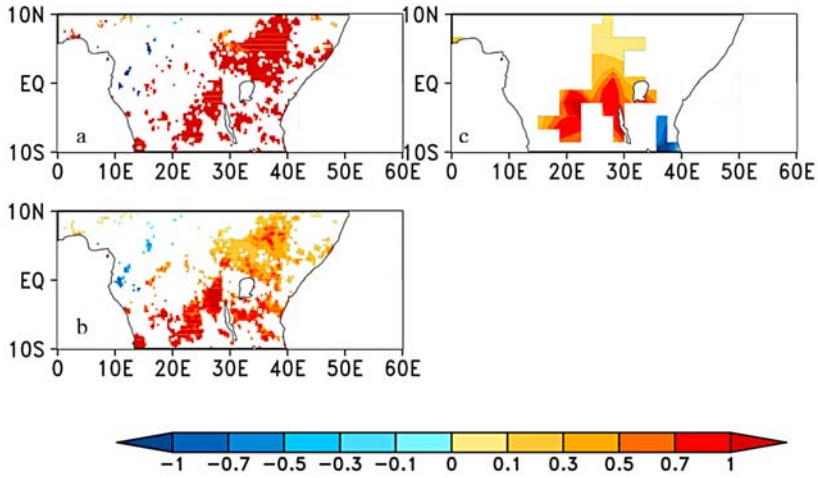

Figure 5. The contemporaneous regressions of the DJF seasonal mean diurnal precipitation range (computed from 3-hourly data) from (a) TRMM and (c) the CCC model on the normalized Niño3 SST index from HADISST (Figure 5a) and the CCC model (Figure 5c). (b) Same as Figures 5a and 5c except for total DJF seasonal mean precipitation anomalies from TRMM. The units are in mm d^{-1}. The regressions are scaled to one standard deviation of the Niño3 SST index.

precipitation range is used instead of the total precipitation. The seasonal mean diurnal precipitation range is calculated as the seasonal average of the daily diurnal amplitude. The 3-hourly data from the TRMM and the CCC model simulation are averaged over the days and the years separately for each 3 h period to derive a climatological seasonal mean diurnal cycle. We then compute the daily diurnal amplitude as the difference of precipitation between the time of the zenith and the nadir of this climatological diurnal cycle. It may be noted that CRU does not have the temporal resolution to resolve the diurnal variability. Therefore, we resort to TRMM data sets for the analysis here. In Figure 5a, we show the regression of the seasonal anomalies of the diurnal precipitation range (computed using the 3-hourly data) from the TRMM 3B42 data set on the Niño3 SST index. Figure 5b shows the corresponding total seasonal

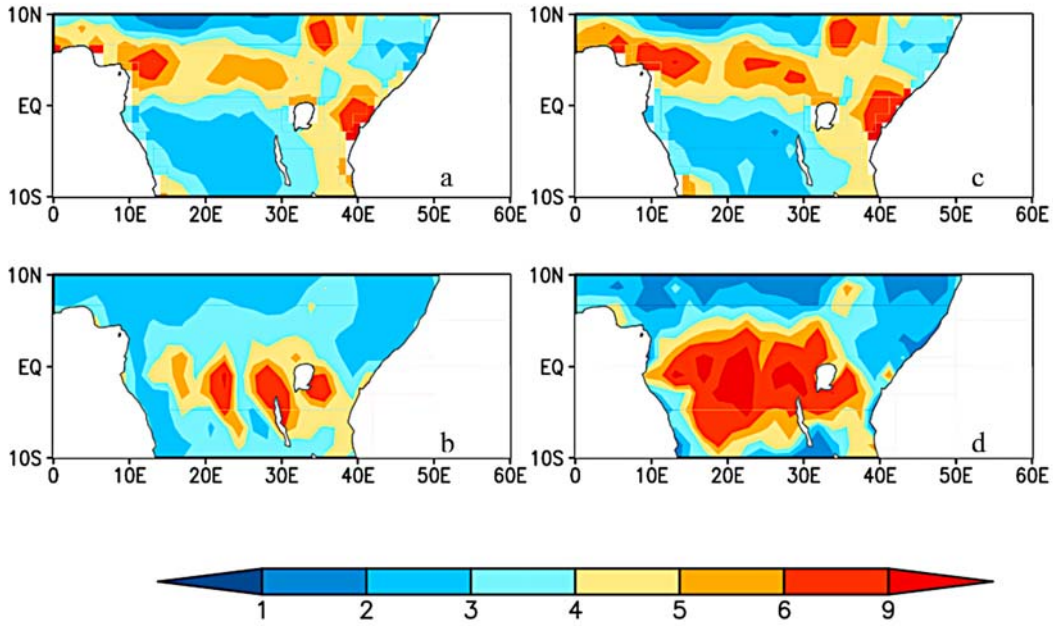

Figure 6. The average decorrelation time of daily precipitation (see text for definition) in the DJF season from (a) GOLD (observations) and (b) the CCC model simulation. The lead time between surface evaporation and precipitation (with positive lags indicating that the former leads the latter) from (c) GOLD and (d) the CCC model simulation. The units are in days. Only significant values at the 90% confidence interval according to the *t* test are shown.

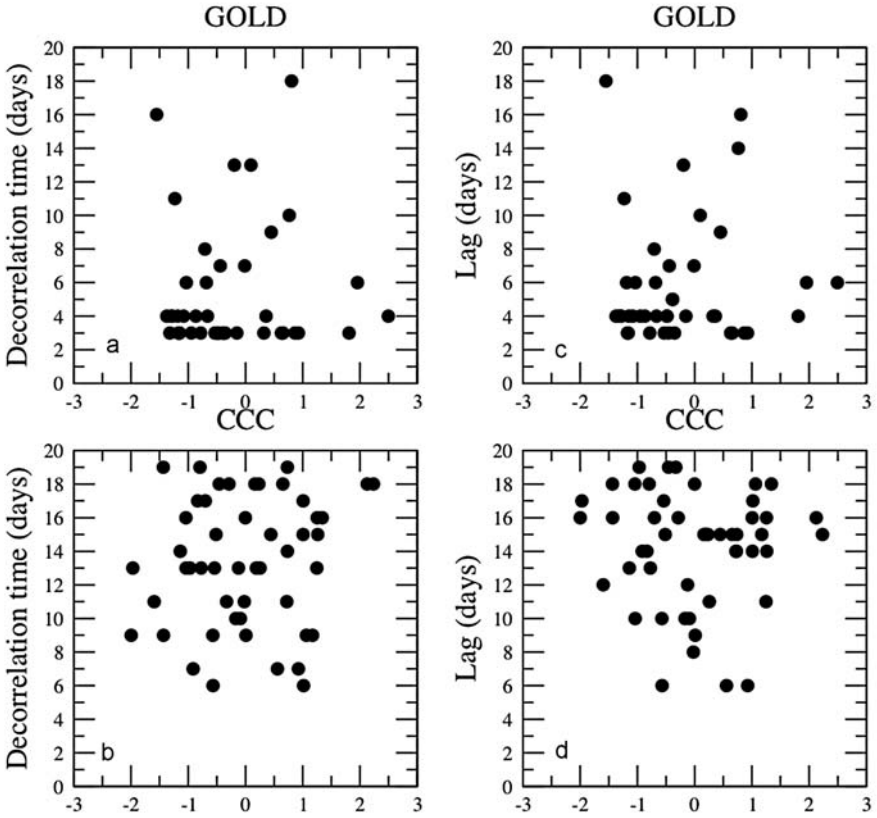

Figure 7. Scatterplot between the DJF Niño3 SST index (in °C) and the corresponding average decorrelation time of daily precipitation over the equatorial Africa region in (a) GOLD and (b) the CCC model simulation. Also, scatterplot between the DJF Niño3 SST index (in °C) and the corresponding lag of precipitation with local evaporation (with the former lagging the latter at positive lags) from (c) GOLD and (d) the CCC model simulation.

mean precipitation from the same TRMM data. Figures 5a and 5b are comparable, suggesting the interannual variations manifest strongly at local diurnal scales over the equatorial African region. The appearance of the anomalies over equatorial Africa in Figure 5b is qualitatively comparable to that obtained in Figure 2a, despite the TRMM and the CRU data sets being two independent sources of data covering different time periods. It may be mentioned that only 8 years (1998–2006) of TRMM data are used here. However, the differences between Figures 5a and 2a are also appreciable. Quantitatively, the TRMM precipitation anomalies in Figure 5b are much larger than the CRU estimates in Figure 2a. Comparing Figures 5c and 2b, the CCC model also displays a similar feature of the interannual variations of the diurnal variability over the equatorial African region. But there are some differences between the TRMM anomalies in Figure 5a and the CCC model anomalies in Figure 5c that point to potential model errors. Essentially, however, these regressions suggest that the diurnal range of precipitation over equatorial Africa is lengthened (shortened) in an El Niño (La Niña) year.

[17] Likewise, the regression of the DJF seasonal mean of the daily diurnal range of precipitation (computed from the 3-hourly data) of the CCC model on the contemporaneous Niño3 SST index is also able to reproduce the teleconnection patterns over equatorial Africa (Figure 5b). In fact, the magnitude of the regression in Figure 5b is larger than in Figure 2b, suggesting that there is some compensatory influence of this interannual signal from atmospheric time scales other than the diurnal variation.

3.4. Mechanism of Scale Interactions

[18] The question asked here is, What is the mechanism by which the remote ENSO forcing interacts with diurnal variability of precipitation over equatorial Africa? The answer to this question lies in the additive influence (or phase locking) of the seasonal cycle, the interannual signal from ENSO, and the local diurnal cycle.

[19] As shown in Figure 1a, the DJF season is the driest season over equatorial Africa. In Figure 2, this seasonal mean precipitation over equatorial Africa varies with SST variations in the Niño3 SST index associated with ENSO. From Figure 2, it follows that a warm (cold) ENSO event would entail a wetter (drier) than normal DJF season over the equatorial Africa region. This interannual variation is also quite apparent in the daily rainfall distribution shown in Figure 4. The CCC model simulation shows that on average in a La Niña year, nearly 15% (50%) of the days in the DJF season have less than 0.1 mm d^{-1} (1 mm d^{-1}). As explained below, such reductions in rainfall in an already dry season will account for a significant reduction in land feedback.

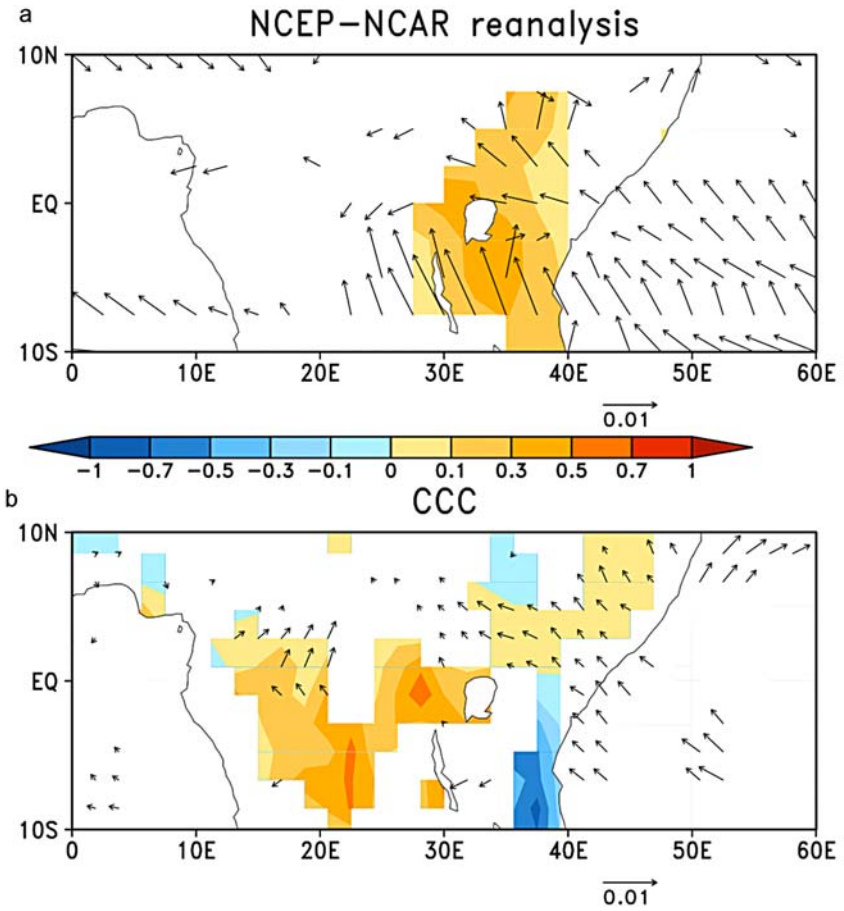

Figure 8. The contemporaneous regression of the DJF moisture flux convergence (shaded; in mm d^{-1}) and moisture flux (in ms^{-1}) at 850 hPa from (a) the NCEP-NCAR reanalyses and (b) the CCC model on the normalized Niño3 SST index from HADISST (Figure 8a) and the CCC model (Figure 8b). The domain of equatorial Africa used in the study is outlined. Only significant values at the 90% confidence interval according to the *t* test are plotted. The regressions are scaled to one standard deviation of the Niño3 SST index.

[20] Figure 6 shows that the land-atmosphere coupling is critical to the maintenance of the precipitation over this region. Following the work of *Misra* [2008], the average decorrelation time of daily precipitation from observations (GOLD data) and the CCC model simulation are shown in Figures 6a and 6b, respectively. This average decorrelation time is defined as the average time in days during the season when the autocorrelation of daily precipitation falls below the significance level according to the *t* test. Both observations and the CCC model show that over the equatorial Africa region, there is an extended memory of daily precipitation that exceeds 4 days. This feature of extended memory of the daily precipitation is sustained by local surface evaporation. This is illustrated in Figures 6c and 6d, which show the average time in days by which the surface evaporation leads precipitation in the GOLD data set and the CCC model simulation in the DJF season. The similarity in the patterns and magnitude between Figures 6a and 6c in the GOLD data set and Figures 6b and 6d in the CCC model simulation clearly indicates that surface evaporation acts as the source for the extended memory of the daily precipitation over equatorial Africa.

[21] In Figures 7a and 7b, it is shown that the area-averaged decorrelation time of daily precipitation over equatorial Africa in the DJF season in the GOLD data set and the CCC model simulation, respectively, does not strongly correlate with the Niño3 SST index variations. Similarly, in Figures 7c and 7d, the area-averaged lead time of evaporation on precipitation over equatorial Africa in GOLD and the CCC model simulation does not change significantly with Niño3 SST index variations. In other words, the ENSO variations do not affect the character or the strength of the existing land-atmosphere coupling over equatorial Africa.

[22] Therefore, in a La Niña year of the driest season of DJF over equatorial Africa, when there is a lack of precipitation, there is a significant positive land feedback from the relatively dry land surface, which further exacerbates the drying at diurnal scales. This is because land-atmosphere positively feeds back to the reducing precipitation at diurnal scales as observed in Figure 5. On the contrary, in an El Niño year, the interannual signal of precipitation is able to mitigate the periodic dryness from the seasonal and diurnal

cycles, thereby showing a larger contrast from a La Niña year over equatorial Africa.

[23] Although the role of the land feedback in the interannual variations of the diurnal variability of equatorial Africa is emphasized, it should be noted that this region of equatorial Africa is transected by the ITCZ, which would suggest that moisture flux convergence would be critical. In Figures 8a and 8b, we show the regression of the vertically integrated (through the depth of the atmosphere) moisture flux convergence and 850 hPa moisture flux (one of the lower levels in the CCC model with high moisture flux) on the standardized Niño3 SST index from the NCEP-NCAR reanalysis and the CCC model integration, respectively. Qualitatively, the results are comparable in the reanalysis and the CCC model with enhanced moisture flux convergence (divergence) in El Niño (La Niña) years over equatorial Africa. Furthermore, the enhanced moisture flux is from the western Indian Ocean in both Figures 8a and 8b. However, there are significant differences between Figures 8a and 8b, with enhanced 850 hPa meridional moisture flux anomalies from the southern latitudes of South Africa in the NCEP-NCAR reanalysis that is poorly simulated in the CCC model. Furthermore, the magnitudes of the moisture flux anomalies are larger in the reanalysis. Significant differences in the moisture flux convergence anomalies are also evident between Figures 8a and 8b. However, the moisture analysis in the NCEP-NCAR reanalyses has often been quoted to be poor, especially in the tropical latitudes [*Karam and Bras*, 2008; *Trenberth and Guiellemo*, 1998; *Mo and Higgins*, 1996].

4. Conclusions

[24] It is shown from observations that the DJF seasonal mean precipitation anomalies over equatorial Africa (20°E–30°E, 6°S–7°N) are strongly associated with the contemporaneous SST variations over the Niño3 region. This interannual variation of precipitation is also reflected at the local diurnal scales over equatorial Africa. Both of these features are captured, at least qualitatively, in a multidecadal integration of the CCC model. This observed feature is investigated further for its mechanism in the model results. It is broadly agreed that such remote teleconnections occur through the formation of atmospheric bridges [*Alexander et al.*, 2002; *Nigam*, 2003], which is confirmed in this case both from the NCEP-NCAR reanalysis and the CCC model integration.

[25] This study shows that the local amplification of the remote ENSO signal over equatorial Africa is a result of the additive influence of the seasonal cycle, the interannual signal, and the local diurnal cycle. The dry season of DJF over equatorial Africa superimposed by the dry signal in a La Niña year causes a severe drying. This leads to a reinforcement of the dry anomalies from the positive land feedback at local diurnal scales, as local recycling essentially sustains the rainfall anomalies over equatorial Africa. In an El Niño year, the wet signal over equatorial Africa mitigates the dry seasonal cycle, which is further sustained by positive land feedback at diurnal scales, and thereby increases the contrast from a La Niña year. This interannual variation of the diurnal variability of precipitation over equatorial Africa is also observed in the TRMM data set.

[26] **Acknowledgments.** The useful input and comments on an earlier version of the manuscript from Sharon Nicholson were invaluable. I also acknowledge two anonymous colleagues for their comments. Meredith Field's expert help in editing this manuscript is also acknowledged. The gracious support of the FSU cornerstone research funds through FYAP and that of the Department of Meteorology is greatly appreciated. This research was supported by NOAA grant NA07OAR4310221. The computing resource of the NASA Advanced Supercomputing (NAS) Division at Ames Research Center under SMD-07-0382 is acknowledged.

References

Alexander, M. A., I. Blade, M. Newman, J. R. Lazante, N.-C. Lau, and J. D. Scott (2002), The atmospheric bridge: The influence of ENSO teleconnections on air-sea interaction over the global oceans, *J. Clim.*, *15*, 2205–2231, doi:10.1175/1520-0442(2002)015<2205:TABTIO>2.0.CO;2.

Bacmeister, J., et al. (2000), An atlas of seasonal means simulated by the NSIPP-1 atmospheric GCM, *NASA Tech. Memo. 104606*, vol. 17, 194 pp., Goddard Space Flight Cent., Greenbelt, Md.

Balas, N., S. E. Nicholson, and D. Klotter (2007), The relationship of rainfall variability in West Central Africa to sea-surface temperature fluctuations, *Int. J. Climatol.*, *27*, 1335–1349, doi:10.1002/joc.1456.

Capotondi, A., A. Wittenberg, and S. Masina (2006), Spatial and temporal structure of tropical Pacific interannual variability in 20th century coupled simulations, *Ocean Modell.*, *15*, 274–298, doi:10.1016/j.ocemod.2006.02.004.

Collins, W. D., et al. (2006), The Community Climate System Model Version 3 (CCSM3), *J. Clim.*, *19*, 2122–2143, doi:10.1175/JCLI3761.1.

Dirmeyer, P. A., and L. Tan (2001), A multi-decadal global land-surface data set of state variables and fluxes, *Tech. Rep. 102*, 43 pp., Cent. for Ocean Land Atmos. Stud., Calverton, Md. (Available at http://www.iges.org/pubs/ctr_102.pdf)

Dirmeyer, P. A., and F. J. Zeng (1999), Precipitation infiltration in the Simplified SiB land surface scheme, *J. Meteorol. Soc. Jpn.*, *78*, 291–303.

Gent, P. R., and J. C. McWilliams (1990), Isopycnal mixing in ocean circulation model, *J. Phys. Oceanogr.*, *20*, 150–155, doi:10.1175/1520-0485(1990)020<0150:IMIOCM>2.0.CO;2.

Giannini, A., M. Biasutti, I. M. Held, and A. H. Sobel (2008), A global perspective on African climate, *Clim. Change*, *90*, 359–383, doi:10.1007/s10584-008-9396-y.

Gill, A. E. (1980), Some simple solutions for heat induced tropical circulation, *Q. J. R. Meteorol. Soc.*, *106*, 447–462, doi:10.1002/qj.49710644905.

Hastenrath, S., A. Nicklis, and L. Greischar (1993), Atmospheric-hydrospheric mechanisms of climate anomalies in the western equatorial Indian Ocean, *J. Geophys. Res.*, *98*, 20,219–20,235, doi:10.1029/93JC02330.

Hayashi, Y. (1980), Estimation of non-linear energy transfer spectra by the cross-spectral method, *J. Atmos. Sci.*, *37*, 299–307, doi:10.1175/1520-0469(1980)037<0299:EONETS>2.0.CO;2.

Hirst, A. C., and S. L. Hastenrath (1983), Atmosphere-ocean mechanisms of climate anomalies in the Angola–tropical Atlantic sector, *J. Phys. Oceanogr.*, *13*, 1146–1157, doi:10.1175/1520-0485(1983)013<1146:AOMOCA>2.0.CO;2.

Hong, S. Y., and H. L. Pan (1996), Nonlocal boundary layer vertical diffusion in a medium range forecast model, *Mon. Weather Rev.*, *124*, 2322–2339, doi:10.1175/1520-0493(1996)124<2322:NBLVDI>2.0.CO;2.

Jackson, B., S. E. Nicholson, and D. Klotter (2009), Mesoscale convective systems over western equatorial Africa and their relationship to large-scale circulation, *Mon. Weather Rev.*, *137*, 1272–1294, doi:10.1175/2008MWR2525.1.

Kabanda, T. A., and M. R. Jury (1999), Inter-annual variability of short rains over northern Tanzania, *Clim. Res.*, *13*, 231–241, doi:10.3354/cr013231.

Kalnay, E., et al. (1996), The NCEP/NCAR 40-year reanalysis project, *Bull. Am. Meteorol. Soc.*, *77*, 437–471, doi:10.1175/1520-0477(1996)077<0437:TNYRP>2.0.CO;2.

Karam, H. N., and R. L. Bras (2008), Estimates of net atmospheric moisture flux convergence over the Amazon Bazin: A comparison of reanalysis products, *J. Hydrometeorol.*, *9*, 1035–1047, doi:10.1175/2008JHM887.1.

Karspeck, A. R., and M. A. Cane (2002), Tropical Pacific 1976–77 climate shift in a linear, wind-driven model, *J. Phys. Oceanogr.*, *32*, 2350–2360, doi:10.1175/1520-0485(2002)032<2350:TPCSIA>2.0.CO;2.

Kiehl, J. T., J. J. Hack, G. Bonan, B. A. Boville, D. L. Williamson, and P. J. Rasch (1998), The National Center for Atmospheric Research Community Climate Model: CCM3, *J. Clim.*, *11*, 1131–1149, doi:10.1175/1520-0442(1998)011<1131:TNCFAR>2.0.CO;2.

Kijazi, A. L., and C. J. C. Reason (2005), Relationships between intraseasonal rainfall variability of coastal Tanzania and ENSO, *Theor. Appl. Climatol.*, *82*, 153–176, doi:10.1007/s00704-005-0129-0.

Krishnamurthy, V., and B. P. Kirtman (2003), Variability of the Indian Ocean: Relation to monsoon and ENSO, *Q. J. R. Meteorol. Soc.*, *129*, 1623–1646, doi:10.1256/qj.01.166.

Krishnamurti, T. N., and D. R. Chakraborty (2005), The dynamics of phase locking, *J. Atmos. Sci.*, *62*, 2952–2964, doi:10.1175/JAS3507.1.

Krishnamurti, T. N., M. C. Sinha, V. Misra, and O. P. Sharma (1998), Tropical-middle latitude interactions viewed via wave energy flux in the frequency domain, *Dyn. Atmos. Oceans*, *27*, 383–412, doi:10.1016/S0377-0265(97)00021-3.

Krishnamurti, T. N., D. R. Chakraborty, N. Cubuckcu, L. Stefanova, and T. S. V. Vijay Kumar (2003), A mechanism of the Madden-Julian Oscillation based on interactions in the frequency domain, *Q. J. R. Meteorol. Soc*, *129*, 2559–2590, doi:10.1256/qj.02.151.

Large, W. G., J. C. McWilliams, and S. C. Doney (1994), Oceanic vertical mixing: A review and a model with a nonlocal boundary layer parameterization project, *Clim. Dyn.*, *18*, 255–272.

Lough, J. M. (1986), Tropical Atlantic sea surface temperatures and rainfall variations in sub-Saharan Africa, *Mon. Weather Rev.*, *114*, 561–570, doi:10.1175/1520-0493(1986)114<0561:TASSTA>2.0.CO;2.

Meeson, B. W., et al. (1995), *ISLSCP Initiative I—Global Data Sets for Land-Atmosphere Models, 1987–1988* [CD-ROM], vol. 1–5, NASA, Greenbelt, Md.

Misra, V. (2008), Coupled interactions of the monsoons, *Geophys. Res. Lett.*, *35*, L12705, doi:10.1029/2008GL033562.

Misra, V. (2009), Harvesting model uncertainty for simulation of interannual variability, *J. Geophys. Res.*, *114*, D16113, doi:10.1029/2008JD011686.

Misra, V., and L. Marx (2007), The manifestation of remote response over equatorial Pacific in a climate model, *J. Geophys. Res.*, *112*, D20105, doi:10.1029/2007JD008597.

Misra, V., et al. (2007), Validating and understanding ENSO simulation in two coupled climate models, *Tellus, Ser. A.*, *59*, 292–308.

Mitchell, T. D., T. R. Carter, P. D. Jones, M. Hulme, and M. New (2004), A comprehensive set of high-resolution grids of monthly climate for Europe and the globe: The observed record (1901–2000) and 16 scenarios (2001–2100), *Tyndall Cent. Work. Pap. 55*, 30 pp., Tyndall Cent., Norwich, U. K.

Mo, K. C., and R. W. Higgins (1996), Large-scale atmospheric moisture transport as evaluated in the NCEP/NCAR and the NASA/DAO reanalyses, *J. Clim.*, *9*, 1531–1545, doi:10.1175/1520-0442(1996)009<1531:LSAMTA>2.0.CO;2.

Moorthi, S., and M. Suarez (1992), Relaxed Arakawa-Schubert: A parameterization of moist convection for general circulation models, *Mon. Weather Rev.*, *120*, 978–1002, doi:10.1175/1520-0493(1992)120<0978:RASAPO>2.0.CO;2.

Mulenga, H. M., M. Rouault, and C. J. C. Reason (2003), Dry summers over northeastern South Africa and associated circulation anomalies, *Clim. Res.*, *25*, 29–41, doi:10.3354/cr025029.

Nicholson, S. E. (1986), The spatial coherence of African rainfall anomalies: Interhemispheric teleconnections, *J. Clim. Appl. Meteorol.*, *25*, 1365–1381, doi:10.1175/1520-0450(1986)025<1365:TSCOAR>2.0.CO;2.

Nicholson, S. E., and D. Entekhabi (1987), Rainfall variability in equatorial and southern Africa: Relationships with sea surface temperatures along the southwestern coast of Africa, *J. Clim. Appl. Meteorol.*, *26*, 561–578, doi:10.1175/1520-0450(1987)026<0561:RVIEAS>2.0.CO;2.

Nicholson, S. E., and J. Kim (1997), The relationship of the El Niño–Southern Oscillation to African rainfall, *Int. J. Climatol.*, *17*, 117–135, doi:10.1002/(SICI)1097-0088(199702)17:2<117::AID-JOC84>3.0.CO;2-O.

Nicholson, S. E., J. Kim, M. B. Ba, and A. R. Lare (1997), The mean surface water balance over Africa and its interannual variability, *J. Clim.*, *10*, 2981–3002, doi:10.1175/1520-0442(1997)010<2981:TMSWBO>2.0.CO;2.

Nigam, S. (2003), Teleconnections, in *Encyclopedia of Atmospheric Sciences*, edited by J. R. Holton, J. A. Pyle, and J. A. Curry, pp. 2243–2269, Academic, Boston, Mass.

Pacanowski, R. C., and S. M. Griffies (1998), MOM3.0 manual, Geophys. Fluid Dyn. Lab., NOAA, Princeton, N. J.

Rayner, N. A., D. E. Parker, E. B. Horton, C. K. Folland, L. V. Alexander, D. P. Rowell, E. C. Kent, and A. Kaplan (2003), Global analyses of sea surface temperature, sea ice, and night marine air temperature since the late nineteenth century, *J. Geophys. Res.*, *108*(D14), 4407, doi:10.1029/2002JD002670.

Reason, C. J. C., and D. Jagadeesha (2005), A model investigation of recent ENSO impacts over southern Africa, *Meteorol. Atmos. Phys.*, *89*, 181–205, doi:10.1007/s00703-005-0128-9.

Reason, C. J. C., and M. Rouault (2002), ENSO-like decadal variability and South African rainfall, *Geophys. Res. Lett.*, *29*(13), 1638, doi:10.1029/2002GL014663.

Redi, M. H. (1982), Oceanic isopycnal mixing by coordinate rotate, *J. Phys. Oceanogr.*, *11*, 1443–1451.

Rouault, M., P. Florenchie, N. Fauchereau, and C. J. C. Reason (2003), South east tropical Atlantic warm events and southern African rainfall, *Geophys. Res. Lett.*, *30*(5), 8009, doi:10.1029/2002GL014840.

Rudolf, B., H. Hauschild, W. Reuth, and U. Schneider (1994), Terrestrial precipitation analysis: Operational method and required density of point measurements, in *Global Precipitation and Climate Change*, *NATO ASI Ser., Ser. I*, vol. 26, edited by M. Desbois and F. Desalmond, pp. 173–186, Springer, New York.

Slingo, J. M. (1987), The development and verification of a cloud prediction model for the ECMWF model, *Q. J. R. Meteorol. Soc.*, *113*, 899–927, doi:10.1256/smsqj.47708.

Smagorinsky, J. (1963), General circulation experiments with the primitive equations: I. The basic experiment, *Mon. Weather Rev.*, *91*, 99–104, doi:10.1175/1520-0493(1963)091<0099:GCEWTP>2.3.CO;2.

Tiedtke, M. (1984), The effect of penetrative cumulus convection on the large-scale flow in a general circulation model, *Beitr. Phys. Atmos.*, *57*, 216–239.

Trenberth, K. E., and C. J. Guiellemo (1998), Evaluation of the atmospheric moisture and hydrological cycle in the NCEP/NCAR reanalyses, *Clim. Dyn.*, *14*, 213–231, doi:10.1007/s003820050219.

Xue, Y.-K., P. J. Sellers, J. L. Kinter, and J. Shukla (1991), A simplified biosphere model for climate studies, *J. Clim.*, *4*, 345–364, doi:10.1175/1520-0442(1991)004<0345:ASBMFG>2.0.CO;2.

Xue, Y.-K., F. J. Zeng, and C. A. Schlosser (1996), SSiB and its sensitivity to soil properties. A case study using HAPEX-Mobilhy data, *Global Planet. Change*, *13*, 183–194, doi:10.1016/0921-8181(95)00045-3.

V. Misra, Department of Meteorology, Florida State University, 404 Love Bldg., 1017 Academic Way, PO Box 3064520, Tallahassee, FL 32306, USA. (vmisra@fsu.edu)